DOI: 10.25923/jxrb-a760

Illustrating the Utility of Flexible and Adaptive Scanning Using the NSSL Advanced Technology Demonstrator in CY25

Lead Author: Addison Alford[1]

Contributors: Charles Kuster[1], Kris Tuftedal[2,1], Eliot Morrow[3,4], Anthony Reinhart[1], Caden Berry[2,1], Emily Blumenauer[2,1], Jacob Carlin[1], Willow Phipps[2,1], Terry Schuur[2,1], Brandon Smith[2,1], Jeffrey Snyder[1], Arthur Witt[1], Noah Boeckman[2,1], Christopher Curtis[2,1], Robbie Estes[2,1], Stephen Gregg[2,1], Larry Hopper[1], Igor Ivić[1], Rakshith Jagannath[2,1], Gerald Kunkle[1], Rafael Mendoza[1], Djordje Mirkovic[2,1], Feng Nai[2,1], Cesar Salazar[2,1], Patrick Servello[2,1], Chad Smith[1], Sebastián Torres[2,1], David Warde[2,1], Danny Wasielewski[1], Felicia Woolard[1], Allen Zahrai[2,1], and Noah Zemlin[2,1]

[1]NOAA/OAR/National Severe Storms Laboratory; Norman, OK; [2]Cooperative Institute for Severe and High-Impact Weather Research and Operations, University of Oklahoma; Norman, OK; [3]Iowa State University, Ames, Iowa; [4]NOAA Ernest F. Hollings Scholarship Program, Silver Spring, MD

Date of Submission: 26 May 2026

Date Accepted for Publication: 15 July 2026

U.S. Department of Commerce
National Oceanic and Atmospheric Administration
Oceanic and Atmospheric Research
National Severe Storms Laboratory

Contents

1. Executive Summary

Dual-polarization phased-array radar (PAR) technology is currently being investigated as a potential tool for weather observations by the National Oceanic and Atmospheric Administration's (NOAA's) National Severe Storms Laboratory (NSSL) in collaboration with the Cooperative Institute for Severe and High-Impact Weather Research and Operations (CIWRO) at the University of Oklahoma. Past research has demonstrated that PARs provide advantages when observing rapidly changing weather because the technology allows meteorologists to observe a full vertical picture of a thunderstorm in 1–2 minutes. While these temporal benefits are significant, dual-polarization PAR has been the subject of intense research recently because as the radar beam is electronically steered away from the center of the field of view, biases occur in the dual-polarization radar variables. To address this dual-polarization PAR challenge, NSSL, along with public and private partners, built the Advanced Technology Demonstration (ATD) PAR in the mid-2010s to investigate if a reliable calibration method can be determined. Results of this work show that dual-polarization PARs can be well calibrated, which results in no meaningful biases as the beam is electronically steered across the field of view.

With substantial progress made in dual-polarization PAR calibration, the ATD has been heavily used for weather observations since 2023 with a strong focus on examining the temporal benefits of PAR. In 2025, NSSL and CIWRO meteorologists collected 170 hours of data that have been used to further examine the benefits of 1–2 minute updates at all elevation angles and/or enhanced vertical coverage (e.g., additional elevation angles compared to operational radar scanning strategies) for weather observation. These data have not only been used to gain insight into severe weather processes, but also provide a demonstration of potential concepts of operation to inform the National Weather Service (NWS) of potential PAR benefits as it steps toward replacing the operational weather radar network.

A main focus of the 2025 data collection was exploring the advanced concepts of operation that stationary PARs enable through the use of Adaptive Focused Observations (AFO). Specifically, an algorithm termed the Adaptive Digital signal processing Algorithm for Phased array radar Timely Scans (ADAPTS) was installed for meteorological use on the ATD in Calendar Year 2025 (CY25). ADAPTS automatically detects weather echoes and only enables beam positions (in azimuth and elevation) in a scanning strategy where significant weather echoes are present. The remaining beam positions without significant weather are not scanned (unless new convection is detected or storms move into formerly weather-free regions), which results in faster radar update times. This report heavily examines the use of ADAPTS for weather observations. We quantify the benefits of ADAPTS in terms of faster scanning without a degradation of coverage or data quality. We explore the benefits of ADAPTS for research observations to further understand severe convective processes, as well as the potential operational benefits in terms of severe hazard detection. We also summarize the flexible scanning capabilities afforded by PAR that have been and are being developed on the ATD, including the development of software tools that may inform future operational practices.

2. Background and Motivation

NSSL has a storied legacy in pioneering new weather radar technologies. Since the mid-2000s, a focal point of NSSL has been on developing and understanding PAR technology for use in weather observation. From the mid 2000s through the mid 2010s, NSSL used a SPY-1A PAR loaned from the United States Navy, which was a single-polarization PAR (e.g., Zrnić et al. 2007, Heinselman et al. 2008). However, the upgrade of the operational Weather Surveillance Radar - 1988 Doppler (WSR-88D) systems used by the NOAA NWS spurred NSSL to begin exploring dual-polarization PAR. In the late 2010s, the ATD PAR was installed in place of the former SPY-1A system (Torres and Wasielewski 2022) as a tool with which to develop, research, and demonstrate dual-polarization PAR.

Currently, the NWS is considering potential replacement options for the aging WSR-88Ds. An Analysis of Alternatives (AoA) is ongoing in which PAR is an option for inclusion as part of the future radar fleet. In order to assist in this analysis effort, NSSL has used the ATD to demonstrate several critical advantages of PAR:

1. Historically, dual-polarization PAR has not been utilized operationally, in part due to the challenge of calibrating a dual-polarization PAR antenna (e.g., Ivić 2020). As the beam is directed off broadside (the direction normal to the face of a PAR antenna), cross-coupling between the horizontal and vertical transmitted waves induces biases in dual-polarization measurements as a function of both azimuth and elevation. Work with the ATD has demonstrated that dual-polarization calibration of a PAR system is achievable and stable over time (Ivić 2023, 2024).
2. Given the success of the ATD's dual-polarization calibration in the early 2020s, attention was turned to using the ATD to collect meteorological datasets to study PAR-specific benefits for weather observation. These efforts accelerated rapidly in 2023. In CY23, attention was paid to observing severe and hazardous weather with the ATD by employing scanning strategies with excellent (relative to currently employed, operational scanning strategies) vertical coverage (i.e., the elevations included in a scanning strategy) that maintained rapid updates (around 90 s in CY23) at all elevations (Alford et al. 2024). In CY24, scan design was shifted to examine the potential benefits of ~1-minute updates by strategically reducing the dense vertical coverage used in CY23 (Alford et al. 2025a). Regardless of the exact number of elevation angles and update times, it

was shown that rapid updates (relative to current operational radar update times) were able to detect important meteorological features faster, provide a more holistic overview of rapidly evolving hazards at all levels, and can offer quantitative benefits to derived information such as quantitative precipitation estimation.

3. Another key goal of data collected in CY24 was to explore the potential of flexible scanning enabled by PAR (Alford et al. 2025a). Unlike mechanically driven radar systems, PAR can nearly instantaneously change the beam direction, providing the means to efficiently collect scans not traditionally used in operations, such as range-height indicators (RHIs), or the inclusion of scans in different transmission modes (e.g., horizontal transmit and simultaneous reception in both polarizations to measure Linear Depolarization Ratio; LDR) whether by RHI or in plan position indicator (PPI) mode. In general, these types of scans, particularly the direction of an RHI, were ATD operator-driven. RHIs afford a detailed and almost instantaneous view in the vertical dimension of severe storms and only take 1–3 s per azimuth to capture, effectively providing no interruption to the more traditional PPI-based scanning strategies.
4. Finally, AFO is a technique to automatically *adapt* the scanning strategy of a radar to the existing weather within its observable range. A form of AFO is implemented in the WSR-88D systems called the Automated Volume Scan Evaluation and Termination (AVSET) technique. AVSET eliminates elevation angles above 5° when no weather echo is present. AFO techniques can be much more sophisticated than eliminating entire elevation angles and are *most* advantageous to implement on a PAR system. AFO was implemented on the SPY-1A system through a technique called ADAPTS (Torres et al. 2016). This algorithm automatically enables beam positions in the direction of significant meteorological echo and disables beam positions in the direction of clear air echo. In CY24, ADAPTS was under development on the ATD system.

3. Data Collection Priorities in CY25

Although much insight was gained from CY23–24 in terms of rapid update benefits, volume coverage, and flexible scanning enabled by PAR, CY25 attention turned to applying AFO to ATD observations.

3.1 Approaching Optimal Scanning Strategies

CY25 data collection priorities were designed to strike a balance between the overarching objectives of CY23 and CY24 by employing PAR-enabled techniques that matured on the ATD system in CY25. Specifically, our overarching aim was to ***observe***

severe and high-impact weather events with dual-polarization PAR by targeting "optimal" scanning strategies that were balanced across data quality, coverage, and update time. Observational strategies that leveraged the flexibility of the ATD, including adaptive scanning, were sought to provide optimal balance in the aforementioned scan attributes.

ADAPTS V (Torres et al. 2026) was released for meteorological use on the ATD in early CY25. Like its predecessor that was used on the single-polarization, SPY-1A system, the algorithm is designed to first check all beam positions in a pre-defined scan definition (i.e., all azimuth and elevation positions in a complete radar volume). However, ADAPTS V incorporates the use of dual-polarization data in its logic unlike the original SPY-1A-based implementation. Through carefully tuned, multi-variable thresholds, beam positions are disabled if no significant meteorological echo is detected anywhere along the radial. In regions of significant meteorological echo, a buffer (or neighborhood in azimuth and elevation space) is included to account for storm growth, evolution, and movement. At regular time intervals (5 minutes during CY25, but can be changed), disabled beam positions are re-checked through very quick "detection beams" that use a low number of pulses (12 ms dwell times per beam position as opposed to 35-60 ms for more standard dwell times) to estimate radar variables and therefore minimize the temporal delay between actual meteorological measurements. The detection beam data are not included in the final radar volume files.

With the ADAPTS V algorithm in place on the ATD, several considerations were levied to develop an observational approach to implement "optimal" scanning strategies:

1. Basic scan definitions were, as in CY23–24, created to fit the predominant meteorological hazard. For example, supercell definitions prioritize low-level revisits and elevation angles as well as hail growth zone elevations with enhanced coverage (meaning added or carefully distributed elevation angles), whereas mesoscale convective system scans de-prioritize mid- and upper-level coverage in favor of enhanced low-level vertical coverage.
2. Basic scan definitions were built assuming that *all* beam positions would be sampled. As such, a maximum scan time of about 90-s, similar to CY23 (Alford et al. 2024), was chosen for most cases. We note that in many scan definitions, revisits at the lowest elevation angle were incorporated to ensure sub-one-minute detections of important tornado-related radar features, such as tornado debris signatures.
3. Relative to CY24 (Alford et al. 2025a), the reduction of elevation angles in a scan definition was not as prevalent, since the goal was not to *always* achieve 1-minute radar volume updates.
4. To achieve 1-minute updates on a more routine basis, ADAPTS V was enabled in almost every case collected in CY25. This afforded "optimization" of scanning strategies, since regions of non-significant meteorological return were

deprioritized, and often saved a significant amount of time. We further quantify the actual time savings afforded by ADAPTS V in section 5.1.

In summary, the use of AFO in the form of ADAPTS V enables optimal scanning strategies by *often* increasing revisits at all elevation angles via automatically disabling beam positions in a pre-defined scan definition. Even in a “worst case” scenario where significant meteorological return occupies the entire azimuth-elevation space of a scan, a ~90-second update at all elevations and ~45 second 0.5° updates still occurs.

3.2 Observing Objectives

Like in CY24, the capabilities of the ATD, specifically the maturation of the ADAPTS V algorithm, enabled several objectives to be explored through routine data collection. Many of the following objectives extend from CY23–24, but consider the novel use of the ADAPTS V algorithm.

3.2.1 Advanced Scanning Concept of Operations

A primary objective of ATD data collection was to demonstrate advanced scanning concepts like ADAPTS in a semi-operational setting. In CY23, the majority of ATD operations were focused on using a PAR system in a very similar manner to current operational systems, wherein scan definitions were largely based on PPIs (horizontal scanning) in a rapid-update framework. In CY24, additional flexibilities were implemented into data collection strategies, including the use of RHIs and the exploration of using LDR transmission. Such concepts of operation were continued in CY25 with the added (and automated) benefit of ADAPTS. Through a series of rigorous engineering tests (Torres et al. 2026) and collaborations with ATD meteorologists in late CY24 (Alford et al. 2025a) and into CY25, the ADAPTS algorithm was determined to be a robust approach to AFO. Upon its *operational* implementation on the ATD in CY25, attention was turned to understanding how AFO with a PAR may provide observational benefits, particularly in terms of rapidly evolving severe weather. We summarize the benefits of ADAPTS in Section 5.1.

3.2.2 Continued Severe Weather Research

As in previous CYs, the exploration of severe weather processes was a primary objective in CY25. Continued observations of tornadoes, hail, severe wind storms, and heavy precipitation were targeted to gain insights into microphysical and kinematic processes attendant to such hazards. The natural benefits of rapid-update low-level and volumetric data, combined with AFO and flexible scanning such as LDR transmission and targeted RHIs, were leveraged to capture novel datasets with which to address core NSSL science objectives. We summarize the initial results of some of these explorations in Section 5.2.

3.2.3 New Techniques

Finally, each iteration in the development and maturation of ATD capabilities affords the opportunity to consider more advanced algorithms and techniques that may be operationally relevant or enhance the research capabilities of the system. This fundamental objective requires close collaboration between hardware and software engineers as well as end-user meteorologists. Although this document heavily focuses on employing the PAR-enabled techniques to collect meteorological observations, we briefly summarize the efforts to inform the continued development of advanced techniques from a meteorological perspective that may be relevant to a potential future operational PAR system.

4. CY25 Dataset Overview

The CY25 dataset led to significant progress relative to the previous two years of ATD data collection. In addition to the implementation of AFO on the ATD system, a fortuitous year of weather events combined with creatively designed tools for use by ATD operators provided the means to collect the most data in any CY since the ATD reached its initial operating capacity. A record 170 hours of meteorological data were collected across 48 separate events throughout the year (Fig. 1). Like in previous years, the ATD was used to capture a wide variety of severe and non-severe weather events. In addition to the expected tornadic supercells, severe mesoscale convective systems (MCSs), and hail-producing thunderstorms climatologically favored in central Oklahoma, the ATD also observed close-range wild fire smoke plumes on 14 March and several winter weather events.

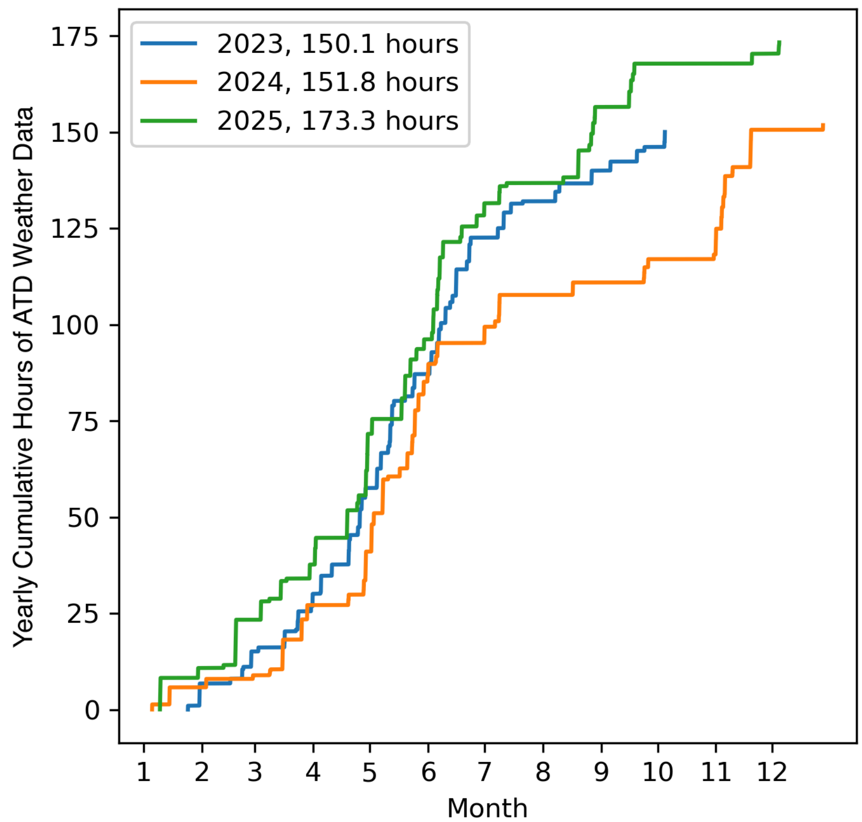

Figure 1. The number of hours of meteorological data collected by CY is shown as a function of calendar month on the x-axis. The legend shows the cumulative total hours per year of data collected.

5. Demonstrating the Benefits of PAR in CY25

In previous CYs, ATD data collection reports (Alford et al. 2024, 2025a) have strongly focused on the benefits of rapid-update data and enhanced or strategically refined vertical coverage gained by using PAR observations. Again, these benefits were evidenced by the data collected in CY25, but we largely focus on the use of ADAPTS V and other flexible scanning modes to demonstrate some of the insights gained into advanced scanning concepts enabled by PAR observations.

5.1 Meteorological Insights Gained from Adaptive Focused Observations

As described in Section 3.1 and detailed in Torres et al. (2026), ADAPTS aims to reduce the total time it takes for one volume scan to complete by only enabling radar beams within a pre-defined volume scan that are in the direction of significant weather echo. In effect, this provides the means to capture faster update data at all elevations of a volume scan, particularly when significant weather echo only occupies a fraction of the ATD's 90° field of view. ADAPTS was enabled for a vast majority of weather collections (see Appendix 1) during CY25, providing the opportunity to measure both the magnitude and frequency of time savings enabled by the ADAPTS algorithm.

The quantitative benefits of ADAPTS were measured across the entirety of CY25 first by computing the total volume time (in seconds) as a function of the maximum elevation angle in a radar volume. This measure roughly assumes that there is a positive relationship between the radar volume time and the top elevation angle of a volume such that more beam positions are likely to be active. We chose this measure as a way to estimate the time savings afforded by ADAPTS without the direct knowledge of the total time each volume *could* have taken, as that metric is not written to individual radar volume files. The maximum volume scan time for most pre-defined scans employed by the ATD during CY25 had a maximum of 90–100 s when all beam positions were active (with the possible reasons for all beam positions being active explained next).

Figure 2a displays the total volume time of all PPI-based volumes taken during CY25 by the ATD. We identified three approximate volume time regimes. The first was radar volumes taken during winter weather events, highlighted in red in Fig. 2a. These volumes took anywhere from ~125 to ~180 s, and ADAPTS was generally not active. As in previous years, volume scan times of 120–180 s were deemed to be reasonable for winter weather observations, which are typically slower evolving relative to warm season, severe convection. They took longer due to the increased dwell times per beam position generally desired for winter weather events. The second regime identified was radar volumes ranging roughly from 70–100 s. These volumes were collected during periods wherein ADAPTS was enabled (although there were a few cases where ADAPTS was not enabled, but represent a small percentage of the volumes collected in CY25), but represented little to no time savings relative to the maximum expected volume time of 90–100 s. In this regime, two possible scenarios were identified based on ATD operator reporting:

1. ADAPTS disabled relatively few, if any, beam positions within the ATD field of view because weather echoes occupied a large fraction of the ATD's field of view. This result is expected, particularly during periods, for example, when storms were at close range to the ATD and large storm complexes such as MCSs were being sampled. Note that this means ADAPTS is working as expected and should not be interpreted as a deficiency in the algorithm performance.
2. ADAPTS was in its "full scan" phase (Torres et al. 2026), which is by design. In the first volume scan after turning ADAPTS on, all beam positions are initially enabled to determine the presence of any significant weather echo in the field of view. Based on this first volume, beam positions are enabled and disabled with buffers (neighborhoods) to account for storm motion and growth (see Torres et al.

2026 for a full description) on the next volume scan, which reduces the scan time as expected. Changes in antenna position, for example, also prompt a full scan phase to reevaluate the presence of significant weather echo in the new field of view.

The third and final regime identified was where ADAPTS provided substantial time savings. We chose to delineate the second and third regimes based on a 60-second volume update or less (but note that this boundary is "fuzzy", since ADAPTS is not inactive in the second regime and to depict regions of greater [blue] and lesser [orange] time savings), based on the goal of achieving a 1-minute volume update in CY24 collections (Alford et al. 2025). The boundary between the winter weather and No/Limited ADAPTS regime is not depicted as "fuzzy," since ADAPTS was not employed in the winter weather regime. Within the three regimes identified, several important takeaways are highlighted:

1. As expected, there is a rough positive relationship between the maximum elevation angle in a volume and the total volume update time, but with substantial deviations due to the application of the ADAPTS algorithm.
2. Across the No/Limited ADAPTS and Full ADAPTS regimes, there exists a wide range of maximum elevation angles, indicating that ADAPTS can reduce azimuthal and elevation coverage of a volume scan. Although this result is expected, it is important to highlight that **ADAPTS is not limited to *solely* reducing elevation coverage, whereas current operational AFO algorithms such as AVSET are.**
3. There are a wide range of volume scan times often clustered at a constant maximum elevation angle. These groups represent heavily-employed volume scans that have a defined maximum elevation angle, wherein ADAPTS reduces coverage across the volume scan beam positions, resulting in a wide range of update times. For example, the cluster of volume update times with a maximum elevation angle of ~21° ranges from ~13 s to ~85 s (Fig. 2a). As such, **deep radar volumes with higher maximum elevation angles can be sampled very quickly using the ADAPTS algorithm**.
4. ADAPTS often reduces the volume update time to and below the 1-minute volume update threshold, a target update time with which to evaluate rapidly evolving hazards such as tornadoes (e.g., Kuster et al. 2025) and provide maximum benefits to precipitation estimation (e.g., Blumenauer et al. 2026). However, in order to achieve a 1-minute volume update without the use of AFO, sacrifices in data quality and/or elevation coverage must be employed (Alford et al. 2025). **ADAPTS often affords 1-minute update times *without* sacrificing data quality or elevation coverage.**

Thus far, we have solely focused on the range of outcomes related to the implementation and use of ADAPTS in meteorological observation. We also examined the frequency of reduced volume update times that ADAPTS afforded relative to the expected 90–100-second maximum update time. In Fig. 2b, we present a normalized histogram showing the distribution of volume scan times for the entirety of CY25. The peak in the distribution is between 80–100 s, coinciding with the maximum update time in the majority of the ATD volume scans of ~90 s. However, there are cumulatively more scans between 0–80-second update time, suggesting that the majority of cases in CY25 benefitted from ADAPTS algorithm. Although the very fast scans were relatively few, there were instances identified (and which are discussed in more detail next) where isolated, deep convection was observed with volume updates on the order of 10–20 s.

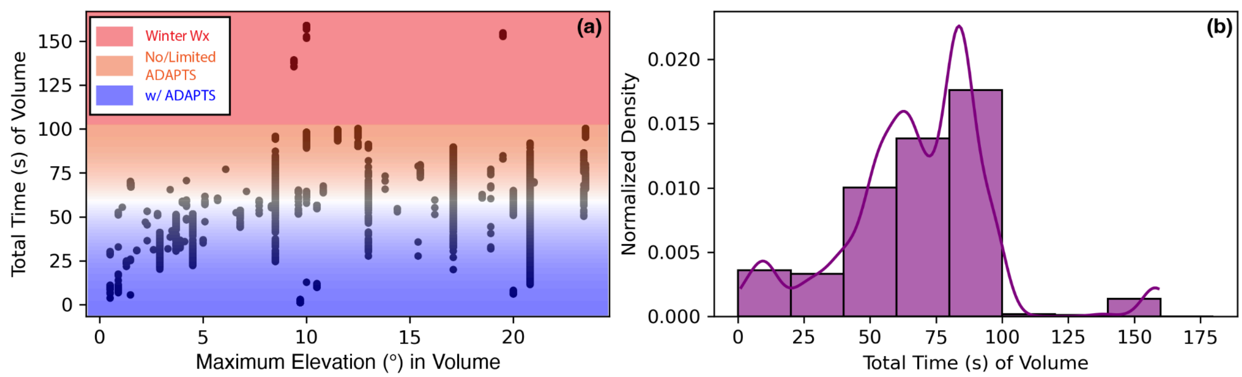

Figure 2. The total time of all radar volumes in CY25 as a function of the maximum elevation reached in the volume is shown in (a). Winter Weather, No/Limited ADAPTS, and ADAPTS categories are drawn with the boundary between No/Limited ADAPTS and ADAPTS being "fuzzy" to depict the less (darker orange) and greater (deeper blue) time savings of ADAPTS. In (b), a normalized distribution as a function of volume duration is shown.

A particularly illustrative example of the benefits of ADAPTS occurred on 18 June, wherein an isolated supercell formed to the southwest of the ATD with very little additional convection initiation in the region. At 2215:05 UTC, a deep scanning strategy with a maximum elevation near 21° was employed and took approximately 85 s to complete with all beam positions enabled. However, the next volume scan (starting at 2216:43 UTC) took 24 s to complete, saving more than 70% of the volume time because ADAPTS identified a minority of beam positions within the pre-defined scan in azimuth-elevation space that the storm in question occupied (Fig. 3).

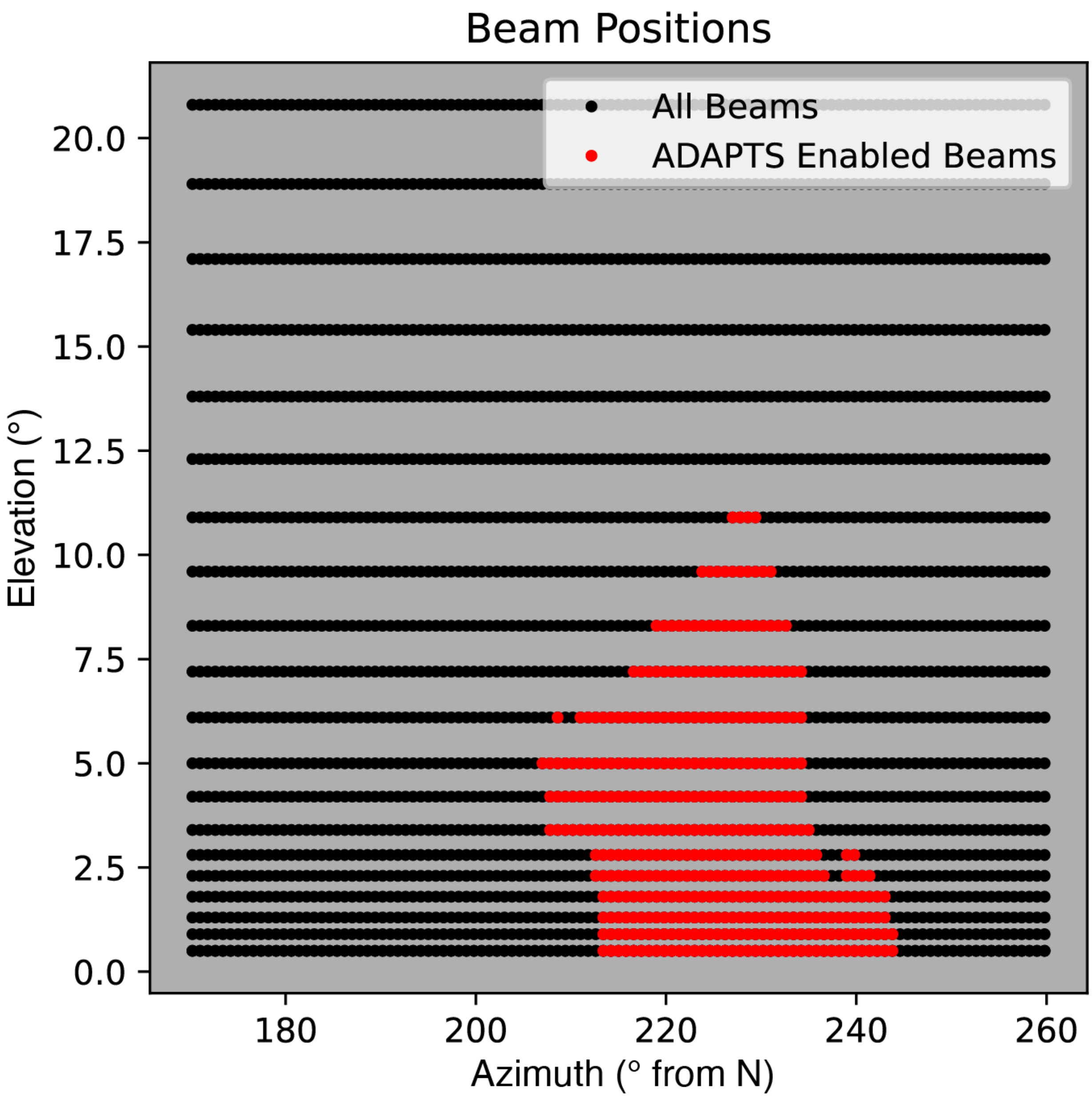

Figure 3. The beam positions sampled during the 18 June 2215:05 UTC radar volume are shown via the “All Beams” category in the black dots. The next radar volume at 2216:43 UTC is shown via the red dots to demonstrate the reduced beam positions retained by the ADAPTS algorithm . Note that the "All Beams" category is meant to convey the coverage of the pre-defined scan without ADAPTS. It can also be interpreted as the beam positions that are disabled by ADAPTS.

We further examined the ATD data from the 18 June case, focusing on the early period in the supercell’s lifecycle prior to the first noted hail reports at about 2223 UTC. As shown in Fig. 4, a hail core identified by the local reduction (between 0–0.5 dB) in differential reflectivity (Z_{DR}) can be seen in the time series. The Z_{DR} reduction appears to begin at 2219:22 UTC (with no indication of a reduction 11 s prior at the 0.5° elevation) on the southwest flank of the supercell. Over the next ~3 minutes, the area of the reduction expands and propagates northeast into the core of the supercell. We note that the update times here, afforded by the ADAPTS algorithm, result in 20–30 second low-level updates, allowing for both the sub-minute spatial evolution of this particular hail core and the Z_{DR} signature's persistence to be evaluated in time.

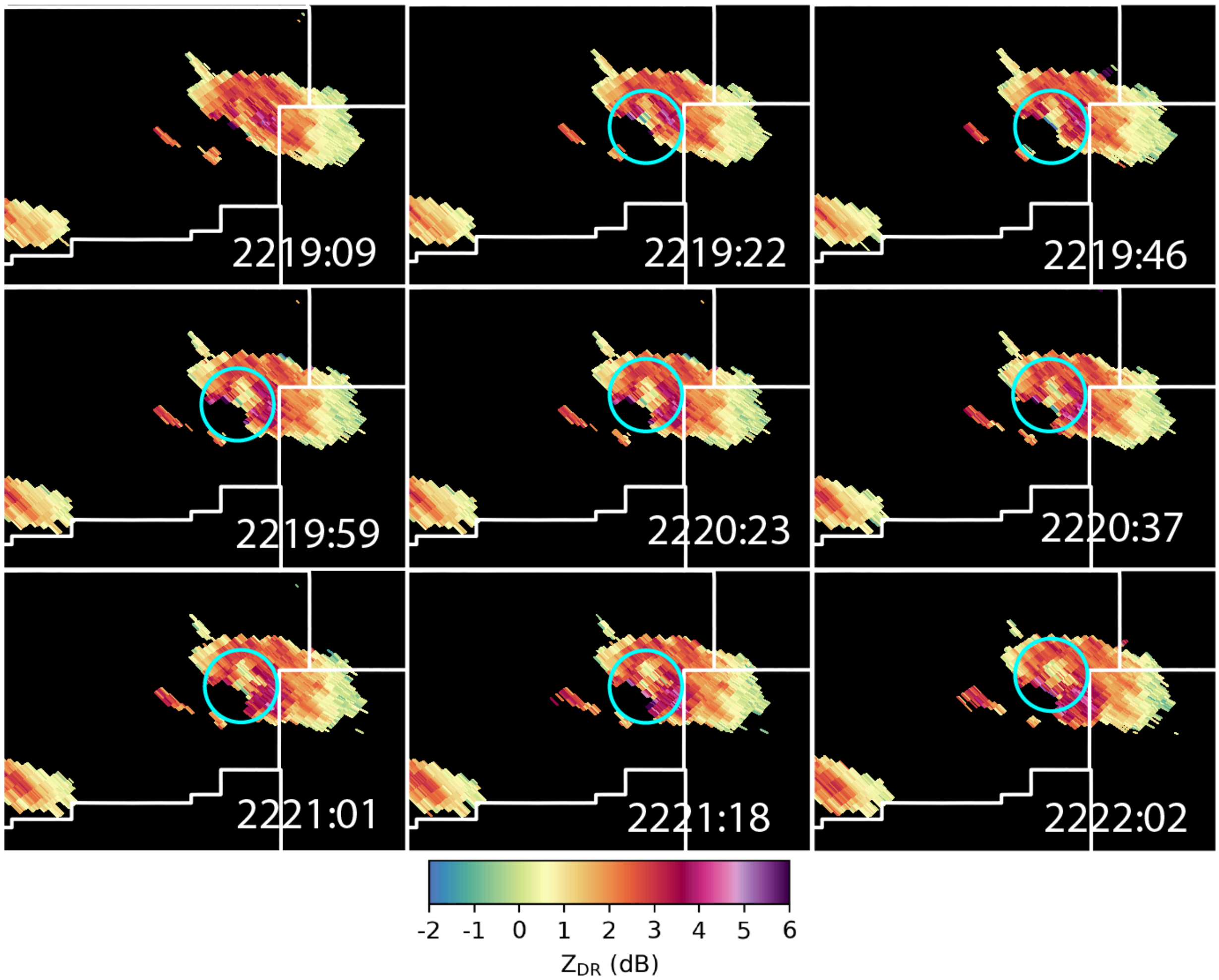

Figure 4. A time series at 0.5° elevation of Z_{DR} according to the color scale from 2219:09 to 2222:02 UTC is shown. The cyan circle is subjectively drawn to draw attention to the reduction in the Z_{DR} on the southwestern portion of the supercell, indicating the presence of a low-altitude hail core.

We likewise examined the evolution of the hail core from a volumetric perspective. We note the scanning strategy employed included non-traditional scans such as true RHIs between "regular" PPI volumes, resulting in the PPI volumes on which ADAPTS primarily acted being separated by approximately 40 s. The PPI volume took about 28 s to complete, followed by a narrow sector of LDR RHIs (7 s) and a low-level LDR PPI (5 s). We reconstructed pseudo-RHIs through the hail core at 228° azimuth, which are displayed in Fig. 5. The radar volume that began at 2219:48 UTC showed an elevated region of high radar reflectivity (Z_H) between 2 and 6 km altitude. Below 2 km, Z_{DR} was on the order of 1.5–2 dB, suggesting mostly rain or small melting hail reaching the surface. However, approximately 40 s later at 2220:25 UTC, the Z_H core had begun descending and a region of lower Z_{DR} was detected below 2 km. Later at 2221:03 UTC, the region of the lowest Z_{DR} had expanded radially in the plane of the pseudo-RHI, coincident with the collapse of the high Z_H core. Although some evolution of the Z_H and Z_{DR} fields *across* the plane of the pseudo-RHI explains the evolution of the hail core in question, the rapid vertical collapse of this particular hail core occurs on timescales much less than typical WSR-88D volume scans. ADAPTS, in this particular case, afforded volume scans that were able to spatiotemporally resolve hail core growth and descent, evidencing its utility in observing rapidly evolving processes.

There are several considerations from an operational perspective that we briefly comment on here:

1. Forecasters in the NOAA Hazardous Weather Testbed (HWT) that have worked with PAR data have noted that volume update times <1 minute may not be necessary for a radar operator to make an informed decision in issuing severe weather warnings (Kuster et al. 2025). It is unclear if a forecaster, when provided ADAPTS data directly, would be able to parse every PPI in every radar volume scan and track individual cores as each scan came in. However, forecasters could make use of sub-minute volume scans to observe such rapidly-evolving trends by looking at loops of the data or leveraging 3D displays of the data. In addition, the use of algorithms that rely on volumetric information to estimate maximum hail size or detect individual hail cores could benefit forecasters by providing concise, digestible information, helping to eliminate the need to directly interrogate every single PPI in a radar volume.
2. Very rapid, low-level update data enabled by ADAPTS, such as that shown in Fig. 4, may offer the most benefit directly to a forecaster, particularly in terms of detecting hail fallout near the surface, monitoring the temporal persistence of low-altitude signatures related to severe hazards, and examining the evolution of rapidly changing features such as tornadoes. Indeed, Kuster et al. (2025) found that forecasters exposed to rapid update data were better able to examine storm-scale evolution when using these data. However, the results described in Kuster et al. (2025) did not include forecaster feedback regarding data collected utilizing ADAPTS. Recent iterations of PAR activities in the HWT have provided forecasters the opportunity to directly examine data collected via ADAPTS. Similar results to the earlier, non-ADAPTS-based studies summarized in Kuster et al. (2025) were found and will be a subject of forthcoming studies.
3. Finally, ADAPTS is but one example of AFO. More advanced concepts of AFO are in development for the ATD and may enable adapting radar observations

(e.g., the distribution and number of elevations in a volume scan) to different storm types and improving data quality, as two examples.

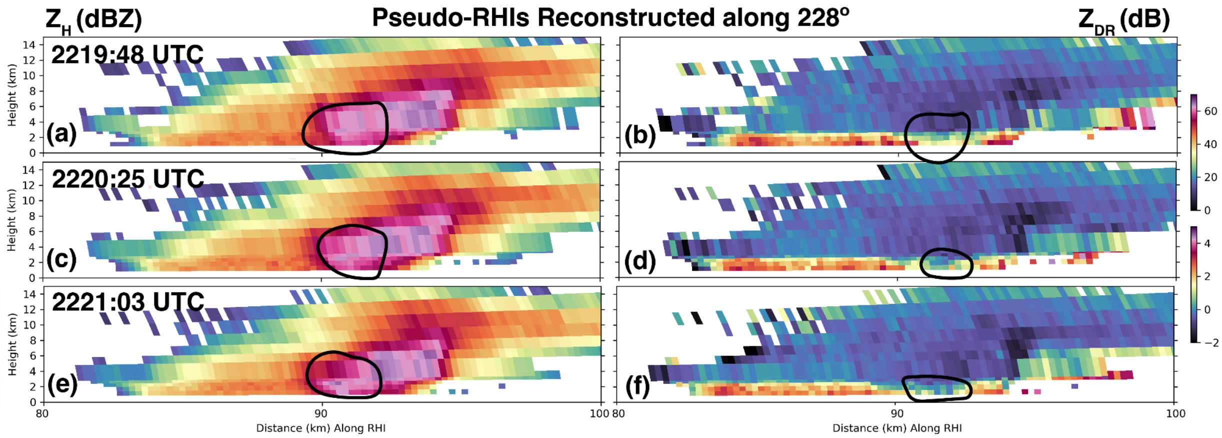

Figure 5. Pseudo-RHIs at 2219:48 (a-b), 2220:25 UTC (c-d) and 2221:03 UTC (e-f) along an azimuth of 228° are shown. Z_H and Z_{DR} are shown in the left and right columns, respectively. A subjectively drawn black contour indicates a region of likely hail fallout seen in the plane of the pseudo-RHI.

5.2 Insights into Severe Weather

As in previous years, the observations collected by the NSSL ATD continue to be leveraged for the purposes of gaining insight into severe weather processes. Key areas of focus include storm-scale processes that influence tornadogenesis (e.g., Alford et al. 2025b), hail size estimation using fundamentals of radar polarimetry (e.g., Carlin et al. 2026, in review), drivers of severe wind production in single- and multi-cell thunderstorms (e.g., Kuster et al. 2021), and heavy rainfall observation and quantification (e.g., Blumenauer et al. 2026). The cases detailed in Appendix 1 represent additional observations that continue to advance these research efforts. We explore one topic in brief to illustrate these efforts.

On 17 May, a supercell thunderstorm (shown early in the observation period in Fig. 6) was observed by the ATD, including observations using the ADAPTS algorithm to decrease volume update time. A maximum update time of about 84 s was expected, but ADAPTS routinely reduced the volume update time during the case to 60-65 s.

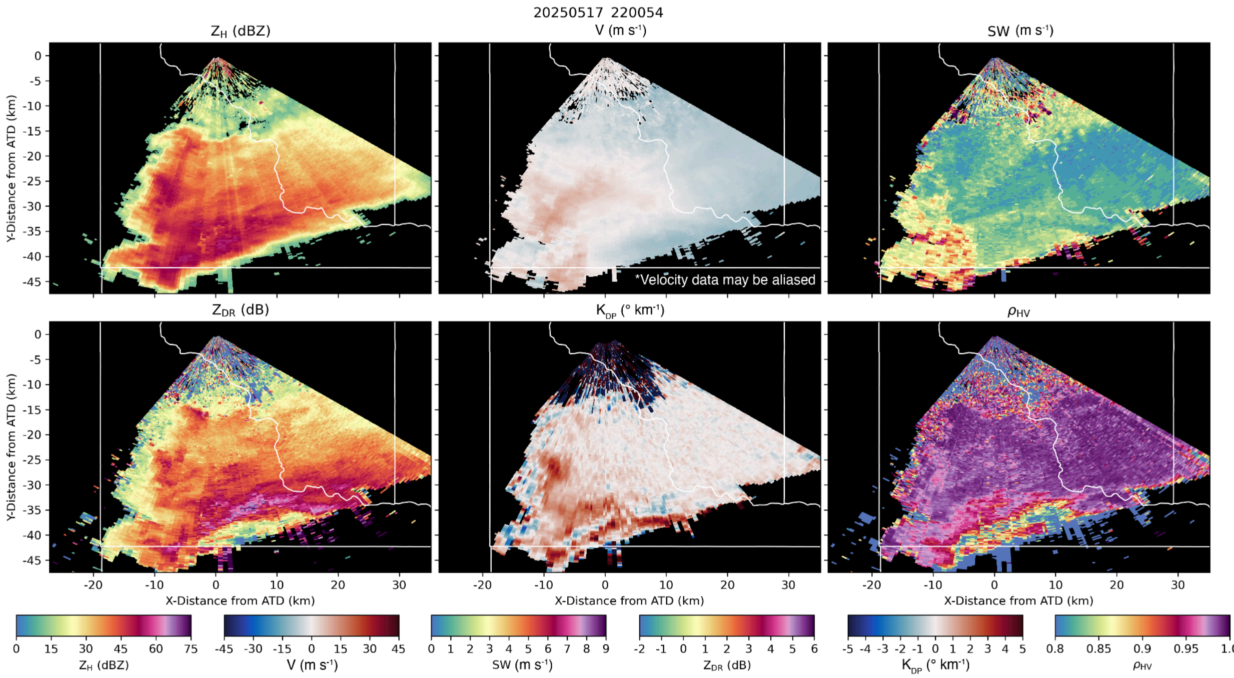

Figure 6. A PPI of a pre-tornadic supercell collected by the ATD at 17 May 2200:54 UTC is shown. On the top row from left to right, Z_H, Doppler velocity, and spectrum width (SW) are shown. On the bottom row, Z_{DR}, K_{DP}, and ρ_{HV} are shown.

As seen in Fig. 6, the southern flank and hook echo-region of the storm was characterized by a strong Z_H gradient. The hook echo-region on the southwest side of the storm was generally not prominent, suggesting that the supercell rear-flank downdraft was weak or the near-surface environment was relatively dry. A 2100 UTC sounding from the NWS in Norman, OK showed a temperature and dew point temperature of 27 and 18 °C, respectively, giving weight to the latter.

An analysis undertaken by a NOAA Ernest F. Hollings Scholar evaluated the pre-tornadic phase of the storm, particularly when the storm displayed little sign of a prominent hook echo feature. Using the analysis technique of Alford et al. (2025b), the mesocyclone center on the 0.5° elevation surface was tracked using the approximate location of the velocity-derived azimuthal shear (commonly referred to as “AzShear”; Mahalik et al. 2019) maximum. Storm motion was computed from the mesocyclone locations as in Alford et al. (2025b). Then, in a 3-km radius from the mesocyclone center, four 90° quadrants surrounding the mesocyclone were partitioned centered on the mesocyclone with the quadrants drawn relative to the mesocyclone forward motion (left and right of mesocyclone motion and “forward” and “rear” of the mesocyclone; see Fig. 7). Data within the 3-km radius were rotated so that the means of dual-polarization data on each elevation surface in each of the four quadrants could be computed. The resulting data, displayed in Fig. 8, is a time-height series of dual-polarization data in the four quadrants relative to the 0.5° elevation mesocyclone center.

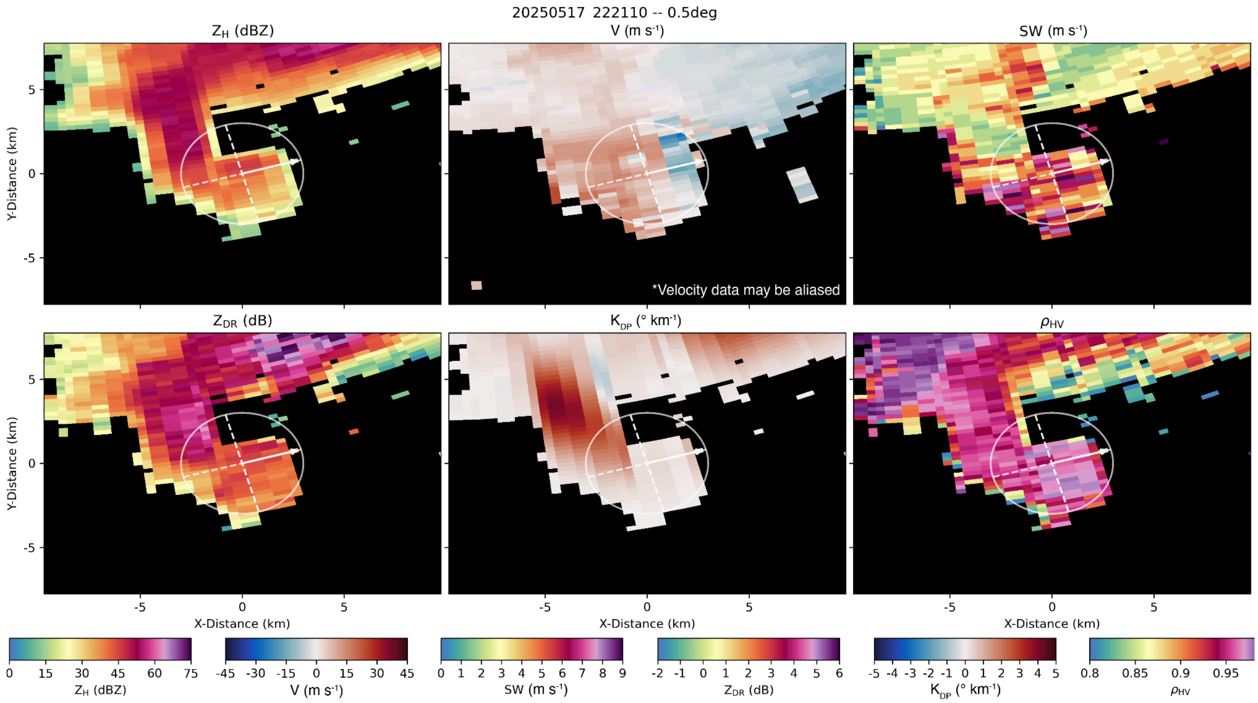

Figure 7. As in Fig. 6, but at 2221:10 UTC. The plots are shown in mesocyclone-relative space with the storm motion vector (arrow pointed north-northeast) and 4 quadrants relative to the motion vector displayed within a 3-km radius.

In Fig. 8, the pre-tornadic evolution of the supercell shown in Fig. 6 is displayed. We particularly focus on the rear-left and rear-right quadrants, as these regions represent the hook echo itself and presumably the rear-flank downdraft region of the supercell. At the beginning of the analysis time, Z_H in all quadrants was minimized near the surface. At the end of the analysis, Z_H began increasing, particularly above 2-km altitude in the rear-left quadrant (i.e., the region of the hook echo that merges with the larger structure of the supercell). We note that for all quadrants, Z_H generally decreases toward the surface. We likewise examine Z_{DR} data in Fig. 9. As a function of height, Z_{DR} tends to decrease toward the surface prior to 2214 UTC in the rear-left quadrant. However, the lower profile of Z_{DR} increases toward the surface after 2214 UTC, particularly nearer tornadogenesis. In terms of the specific differential phase (K_{DP}) shown in Fig. 10, the magnitudes of K_{DP} are quite small in all quadrants. Particularly in the rear-left quadrant, there is a subtle decrease in K_{DP} toward the surface at nearly all times.

Based on the vertical structure of the dual-polarization data in Figs. 9–10, we find that the presence of significant evaporation is likely prior to 2214 UTC. The decrease in Z_H, Z_{DR}, and K_{DP} in a vertical column near the surface suggests that most drops are likely evaporating (Kumjian et al. 2022). In particular, K_{DP} generally less than 0.5° km^{-1} suggests low concentrations of liquid water in the hook echo region and the evaporation of small drops as they fall toward the surface. Decreasing values of Z_H and Z_{DR} near the surface likewise suggests that large drops were also evaporating, implying substantial evaporation and potentially an enhanced temperature deficit in the underlying surface cold pool.

After 2214 UTC, the overall magnitudes of Z_{DR} began increasing, suggesting fewer of the large drops were evaporating and/or larger drops were advecting into the region. In addition, Z_{DR} began increasing toward the surface, particularly in the rear-left quadrant. This signature, however, is more indicative of size sorting rather than evaporation as the dominant observed precipitation process (Kumjian et al. 2022). By 2225 UTC, about 3 minutes prior to tornadogenesis, the drop size distribution shifted toward larger drops in the hook-echo region, indicated by increasing low-level Z_{DR} in the rear-left and rear-right quadrants. In addition, K_{DP} began increasing in the low levels to nearer 1° km^{-1} around 2225 UTC, just before tornadogenesis, suggesting a broader drop size distribution comprising both small and large drops. Although the size sorting signature between 2214-2228 UTC does not entirely exclude the presence of evaporation, the *potential magnitude* of evaporation may have decreased after 2214 UTC, especially with the increase in low-level K_{DP} indicating the reduction in the potential evaporation of smaller drops. In the final few minutes prior to tornadogenesis (2225–2228 UTC), both Z_{DR} and K_{DP} rapidly decrease again, consistent with the results of Tuftedal et al. (2021). The temperature deficit in the surface cold pool is thought to substantially control the likelihood of tornadogenesis in supercells (e.g., Markowski and Richardson 2017), suggesting that examining the full three- and four-dimensional evolution of *volumetric* dual-polarization data may afford the opportunity to more deeply understand the microphysical controls on the surface cold pool evolution.

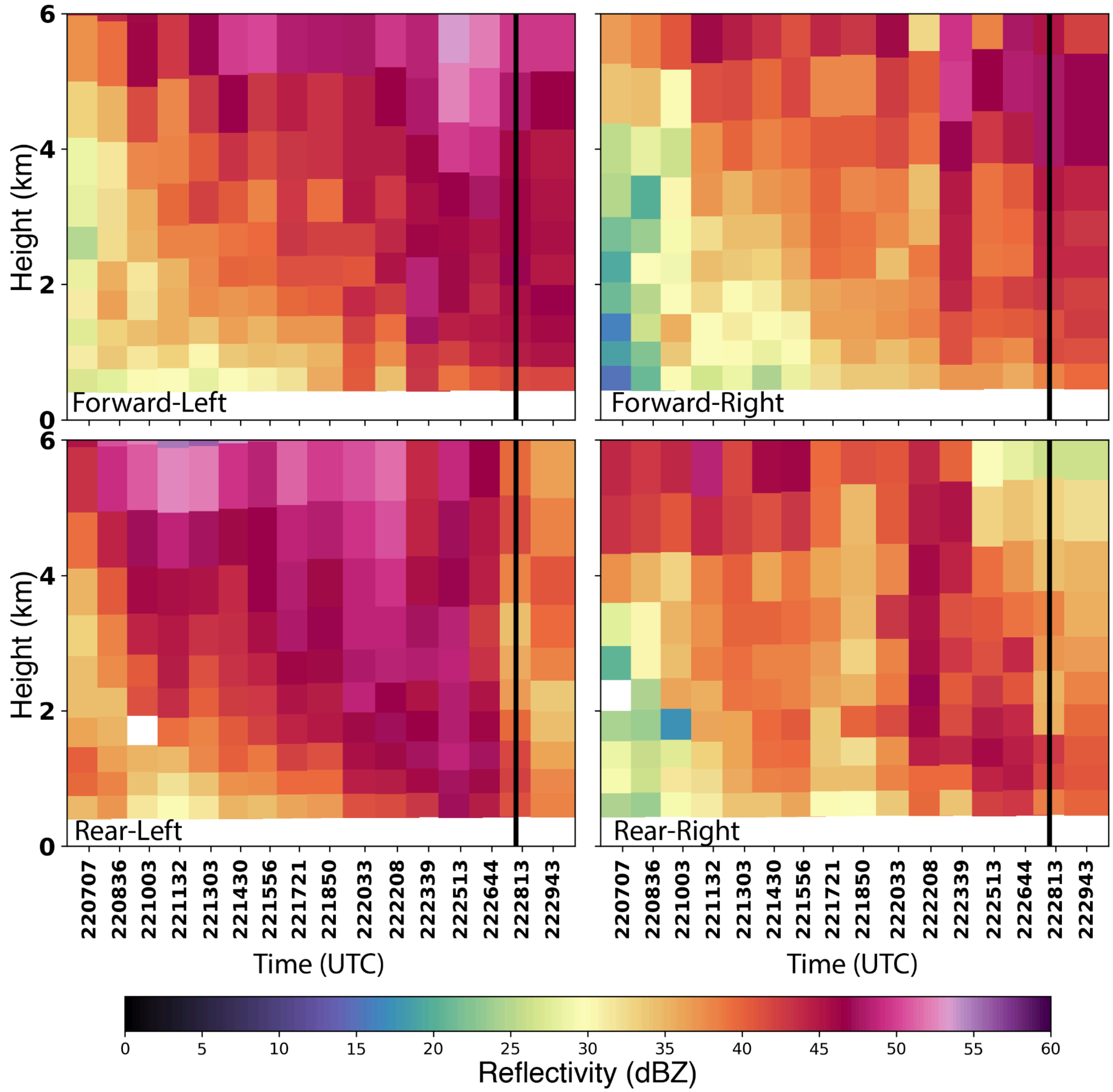

Figure 8. A time-height series of Z_H, averaged in mesocyclone-motion relative quadrants, is shown. The vertical black line at 2228 UTC indicates the time of a confirmed tornado documented by the NWS. White pixels indicate missing data.

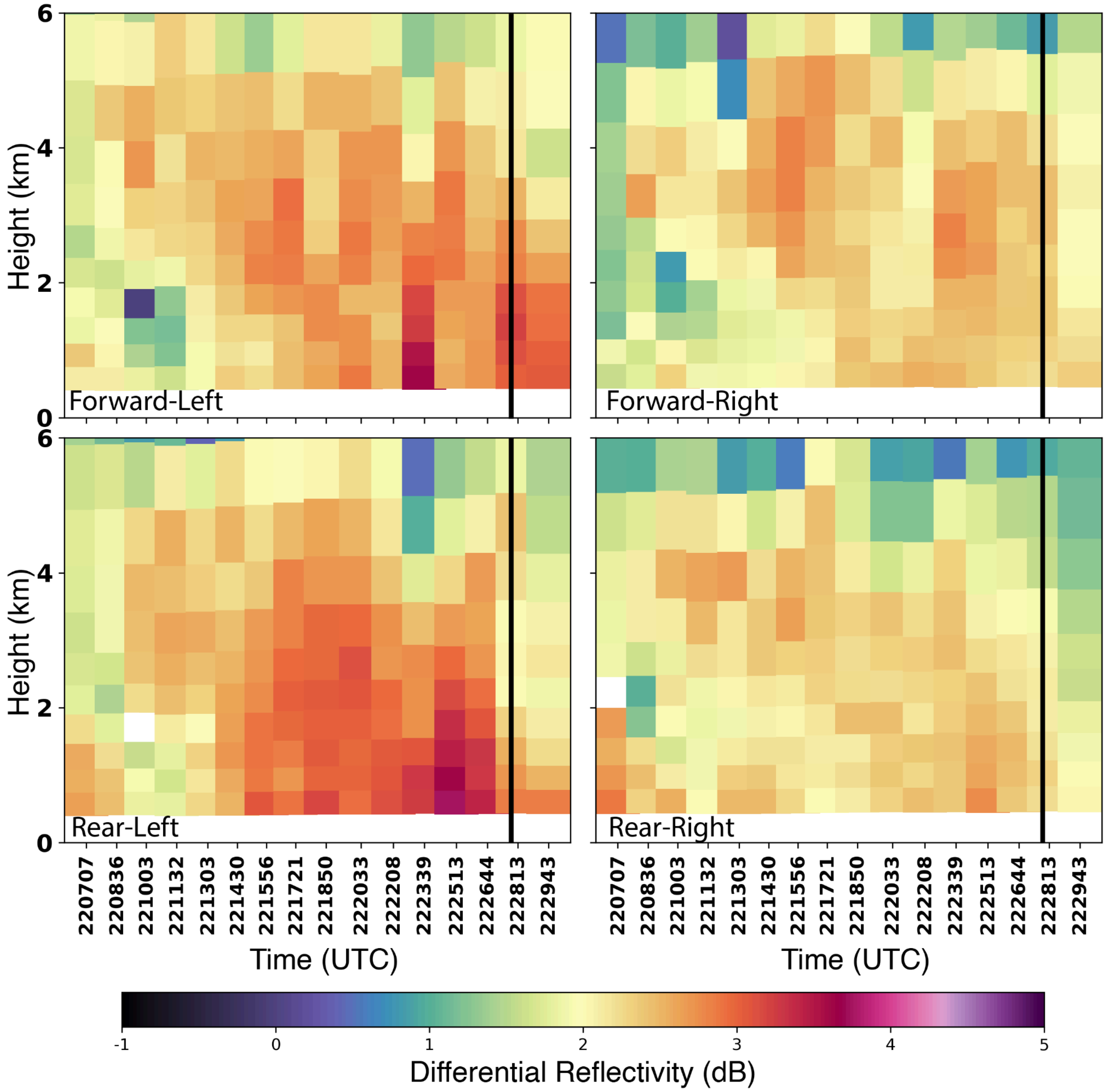

Figure 9. *As in Fig. 8, but for* Z_{DR}.

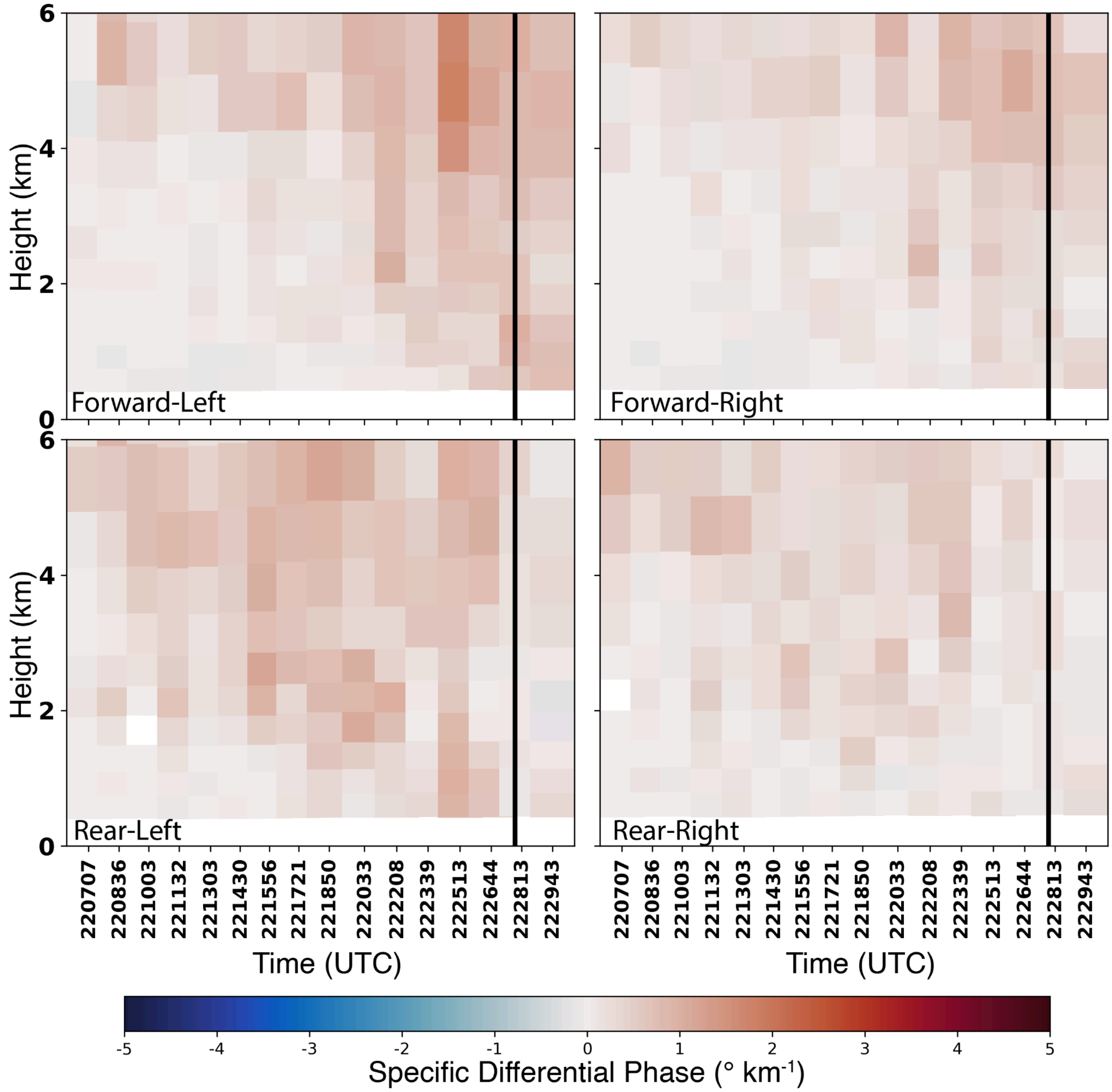

Figure 10. As in Fig. 8, but for K_{DP}.

5.3 Advancing Observations

In past reports, we have described the joint efforts between the meteorological and engineering teams that have targeted the development of tools to enable flexible observations such as RHIs (true RHIs, not to be confused with pseudo-RHIs reconstructed from PPI-based scans) and transmission modes such as LDR and radar imaging (Alford et al. 2024, 2025). The PAR Program not only uses these tools and techniques for severe storms research, but also uses these tools and concepts as demonstrations of the advanced scanning capabilities PAR enables and their potential use in operations.

One particular area that is at a highly mature state is the ability to capture RHI data with the ATD. Although any radar system, including mechanically driven systems, can capture RHIs, PAR enables very efficient RHI scans by instantaneously moving from one scan (e.g., a PPI-based scan) to the RHI with no temporal delay to mechanically decelerate and re-position the antenna. A future operational PAR system *may* wish to allow users to direct targeted RHIs to assess the instantaneous, detailed vertical structure of a severe storm. We document several important takeaways from CY25 data collection that may inform future operational design of RHI scanning on a future system as follows:

1. On the ATD, RHIs are minimally “invasive” to the scanning sequence. The software architecture on the ATD that enables meteorologists to incorporate RHIs into the scanning strategy sequence is termed a “Playlist.” Playlists consist of at least two scanning strategies, frequently combining a full-sector PPI with targeted RHIs.
2. On the ATD, the azimuth along which a single RHI (or the center RHI if multiple RHIs comprise a scanning strategy definition) is taken is, by default, at the broadside angle. In CY23, meteorologists had to reposition the ATD antenna pointing angle to maintain the RHI(s) focus on a target of interest between Playlist cycles. However, repositioning the antenna every few minutes is a tedious task, itself requiring attention that could otherwise be directed to more important tasks. In CY24, updates to the ATD software resulted in “on-the-fly” adjustments to the RHI position that would redirect the azimuthal position of an RHI generally at the beginning of the next Playlist cycle. Effectively, an “on-the-fly” adjustment is a change in the scan definition itself, and the information that is changed (defined by earth-relative beam positions) are updated and sent to the Radar Controller. At the time, however, on-the-fly changes were implemented via a separate dialog window, requiring not only evaluating the desired change in azimuth of the RHI but also iterating through several steps to implement the change.
3. In CY25, ATD engineers creatively designed and implemented a point-and-click version of the on-the-fly adjustment to the RHI position. Effectively, meteorologists can simply direct the next RHI to be taken at some position by mousing over the feature of interest and going through a simple process (on the order of seconds) to change the RHI position. On the ATD, the change takes effect prior to the next iteration of an RHI (or multiple RHIs) in a given Playlist (there is an option to apply the change to all [the default] or some RHIs if there are multiple RHIs in a Playlist sequence).

We highlight this simple (from a user perspective) point-and-click method to direct RHIs, as it is likely relevant for future operational consideration. In discussion sessions during PAR activities in the NOAA HWT (Kuster et al. 2025), forecasters were exposed to potential flexible scanning options such as RHIs. During discussion sessions, the practical implementation of RHIs was discussed, and forecasters largely stated that some sort of “point-and-click” methodology would likely be the most effective. Indeed, during CY25 it was shown that the ATD’s radar control software is capable of accepting on-the-fly changes, which suggests potential future operational systems can easily implement similar methodologies and doing so would have little impact on a radar operator’s workflow.

In past years, we have also highlighted that RHIs afford a near-instantaneous view of severe convection in the vertical dimension. The flexibility of PAR affords the means to collect standard radar volumes via RHI scanning, rather than PPI scanning (i.e., “vertical raster scanning”). To date, including in CY25, a vast majority of the volume data obtained was by collecting PPIs at a constant elevation and constructing a full volume scan through multiple PPIs. On the ATD, a scan definition is simply a series of beam positions as a function of elevation and azimuth. As such, we can transpose the order of the beam positions in a scan to scan vertically at a fixed azimuth and construct a full volume via RHIs from left to right across the ATD field of view (Fig. 11). The scan time and positions of the beams are identical between PPI-based and RHI-based scanning due to the use of electronic beam steering. Nevertheless, this mode of scanning raises practical considerations that are the subject of a joint engineering and meteorological effort to assess, for example, the reconstruction of the RHI-based volume into PPI data for easier viewing of data in a plan view. Likewise, we are considering how best to display vertical raster scanning data in both a real-time viewer and in data packaging. From a strictly meteorological perspective, we aim to address the following questions as this effort moves forward:

- Are there quantitative benefits to products (e.g., vertically-integrated products such as maximum estimated hail size) and other services (e.g., storm-scale data assimilation) to sampling severe and hazardous weather in a nearly-instantaneous vertical framework?
- Are there qualitative and quantitative tradeoffs to end-users such as NWS forecasters to updating a volume (and the individual PPIs) as the RHI-based sampling moves from left to right?
- Although any one storm is still being observed at the same temporal resolution as in a PPI-based volume, are there disadvantages to iteratively constructing a PPI on the time scale of a single radar volume?
- What kind of data packaging is required to view these reconstructed-PPI data using currently available display software, particularly third-party software that is not under our control?

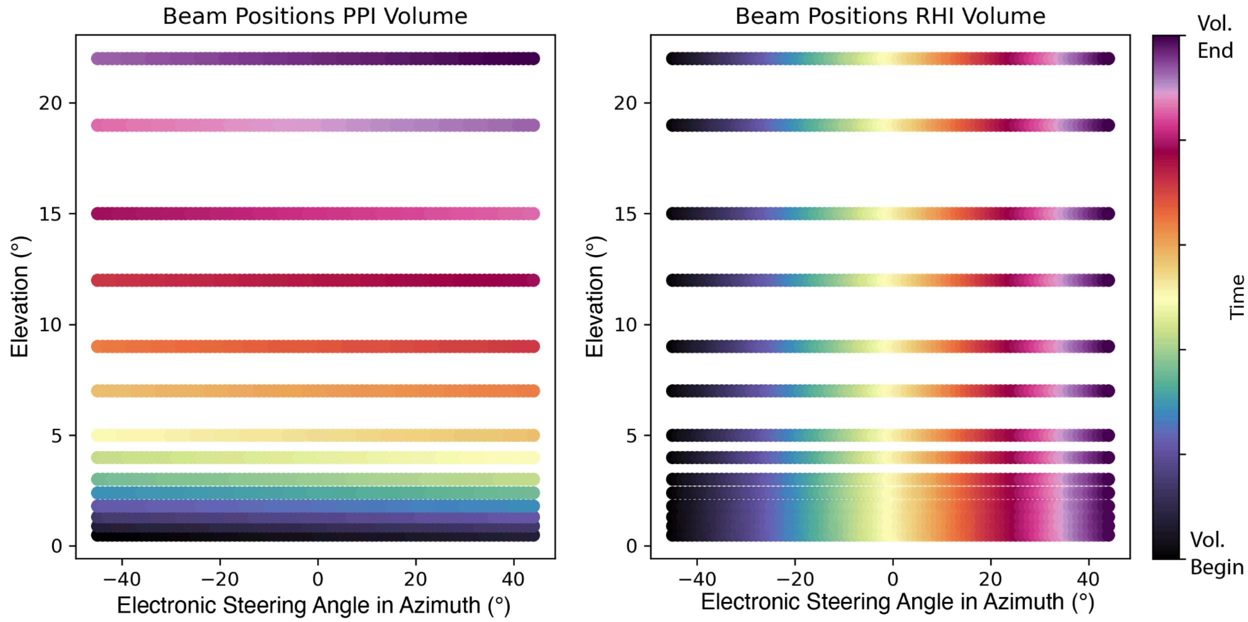

Figure 11. A conceptual model of PPI-based versus RHI-based scanning is shown. The azimuth data are shown relative to one face of a PAR antenna.

6. Discussion

We have briefly reviewed some highlights of ATD data collection from CY25 with a particular focus on how AFO advantages both the operational and research impacts of PAR. We have also summarized some of the collaborations between engineers and meteorologists with a focus on how the development efforts are not only applicable to the ATD itself, but also are a practical demonstration of possible future concepts of operation.

The implementation of ADAPTS on the ATD greatly advances the demonstration of stationary PAR concepts of operation. As shown in Section 5.1, ADAPTS often reduces scan times by 20–40 s. For a scan designed with a maximum update time of 90 s (matching the minimum revisit time of the WSR-88D at 0.5°), this 20–40 s reduction represents a substantial gain. Crucially, these efficiencies are achieved without compromising data quality or vertical coverage, providing a distinct advantage for observing rapidly evolving severe hazards. However, we note that this is not the only form of AFO that may be considered and is solely a first step on the ATD. AFO that first disables beam positions, but uses the time savings (or a portion thereof) to enable better data quality and/or improve coverage (in azimuth and/or elevation) is possible.

We also demonstrated one area of active research that benefitted from the application of ADAPTS. Supercell observations represent one of the fastest-evolving storm modes that can result in rapid-succession cycles of surface hazards (e.g., tornadoes, hail, flooding). In our discussion of the 18 June hail event in southwest Oklahoma and the 17 May tornadic supercell event, we not only examined the near-surface evolution of the hail and (pre-)tornadic hazards, but also the rapid evolution of processes through the observed radar volume. These volumetric data were taken on the order of one minute or less, and substantial changes that relate to changes in storm-scale kinematics and microphysics from volume to volume were demonstrated. For example, the pre-tornadic evolution of the 17 May supercell showed that dual-polarization signatures consistent with substantial evaporation were observed 15–30 minutes prior to tornadogenesis, suggesting the potential for a colder rear-flank downdraft capable of undercutting the supercell updraft and limiting tornadogenesis potential. Later in the observation period, closer to tornadogenesis, such a signature rapidly changed over a few minutes and suggested less evaporation potential, signifying a warmer rear-flank downdraft was possible. Using PAR and ADAPTS together enables viewing the rapid horizontal and vertical changes that occur in supercells and may be potentially helpful to forecasters making real-time assessments of radar-observed supercell structure.

As shown in the 18 June case, ADAPTS enabled very rapid volumes through a rapidly-evolving severe hailstorm. Individual descents of hail cores were visible in the ATD data, which may be useful to forecasters. When we reconstructed pseudo-RHIs (Fig. 5) from even 40-second PPI volumes, there are still visible changes that result from storm advection in the plane of the pseudo-RHIs from the bottom to top elevations that are related to the PPI-based scanning and temporal delay from low to high elevation data. We discussed how flexibly-scanned RHIs on the ATD can enable instantaneous and targeted views of severe convection, which can enable the assessment of updraft structure, microphysical evolution (such as hail), and precise storm-top height measurements if viewed in a time series. However, we note that the temporal delay from bottom to top of a PPI-based scanning strategy can also be eliminated through vertical raster scanning and may provide benefits to storm-scale assessment, research, and data assimilation techniques.

7. Acknowledgements

The authors wish to acknowledge Ted Mansell and Thea Sandmæl for their review of this report and the valuable comments and suggestions that improved its quality. The CIWRO authors on this report were supported by NOAA/Office of Oceanic and Atmospheric Research under NOAA-University of Oklahoma Cooperative Agreement #NA21OAR4320204, U.S. Department of Commerce.

8. List of Acronyms

- AoA — Analysis of Alternatives
- ADAPTS — Adaptive Digital signal processing Algorithm for Phased array radar Timely Scans
- AFO — Adaptive Focused Observations
- ATD — Advanced Technology Demonstrator
- CIWRO — Cooperative Institute for Severe and High-Impact Weather Research and Operations
- CY — Calendar Year
- ρ_{HV} — Correlation coefficient
- HMI — Human-Machine Interface
- HWT — Hazardous Weather Testbed
- K_{DP} — Specific differential phase (in units of degrees per kilometer)
- LDR — Linear Depolarization Ratio
- MCS — Mesoscale Convective System
- NOAA — National Oceanic and Atmospheric Administration
- NSSL — National Severe Storms Laboratory
- NWS — National Weather Service
- PAR — Phased-array radar
- PAMST — Phased Array Meteorological Studies Team
- PPI — Plan Position Indicator
- PRT — Pulse Repetition Time
- QLCS — Quasi-Linear Convective System
- RHI — Range-Height Indicator
- SW — Spectrum Width (m s^{-1})
- TDS — Tornado Debris Signature
- VCP — Volume Coverage Pattern
- WSR-88D — Weather Surveillance Radar - 1988 Doppler
- Z_H — Radar reflectivity (in units of dBZ unless otherwise specified)
- Z_{DR} — Differential radar reflectivity (in units of dB)

9. References

Alford, A. A., and Coauthors, 2024: 2023 Data collection with the NSSL Advanced Technology Demonstrator. NOAA/NSSL Technical Memo, 47pp., doi: 10.25923/4v1r-yq31.

Alford, A. A., and Coauthors, 2025a: Rapid Update, Flexible, and Advanced Scanning Concepts Demonstrated by the NSSL Advanced Technology Demonstrator Phased Array Radar in CY24. NOAA/NSSL Technical Memo, 61pp., doi: 10.25923/ch8h-q184.

Alford, A. A., R. L. Miller, and C. M. Kuster, 2025b: Dual-Polarization Phased Array Radar Observations of Quasi-Linear Convective System Tornadic Mesovortices. *Geophys. Res. Lett.*, **52**, e2025GL115283, doi:10.1029/2025GL115283.

Blumenauer, E., A. A. Alford, D. J. Bodine, P. E. Kirstetter, R. A. Clark, and A. E. Reinhart, 2026: Quantitative Precipitation Estimation with the NSSL Advanced Technology Demonstrator Phased Array Radar. *Geophys. Res. Lett.*, **53**, e2025GL119692, doi: 10.1029/2025GL119692.

Carlin, J. T., Torres, S., A. A. Alford, A. V. Ryzhkov, C. M. Kuster, E. Blumenauer, K. S. Tuftedal, B. Smith, C. Berry, J. Boettcher, C. D. Curtis, R. Estes, S. Gregg, A. E. Reinhart, T. Schuur, L. J. Hopper Jr.: Revisiting the utility of Linear Depolarization Ratio using the Advanced Technology Demonstrator phased array radar. *Bull. Amer. Meteor. Soc.*, in review.

Heinselman, P. L., D. L. Priegnitz , K. L. Manross , T. M. Smith, and R. W. Adams, 2008: Rapid sampling of severe storms by the National Weather Radar Testbed Phased Array Radar. *Wea. Forecasting*, **23**, 808–824, doi:10.1175/2008WAF2007071.1.

Ivić, I., R. Mendoza, D. Schvartzman, S. Torres, and D. Wasielewski, 2020: Preliminary report on polarimetric calibration for the Advanced Technology Demonstrator, NOAA/NSSL report, 34 pp. https://nssl.noaa.gov/publications/par_reports/.

Ivić, I., F. Nai, and S. Torres, 2023: An update on polarimetric calibration for the Advanced Technology Demonstrator, NOAA/NSSL report, 74 pp. https://nssl.noaa.gov/publications/par_reports/.

Ivić, I. 2024: An Overview of the PPAR Advanced Technology Demonstrator Polarimetric Calibration. ERAD 2024 Conference, Rome, Italy, doi: 10.13140/RG.2.2.23343.65442

Kumjian, M. R., O. P. Prat, K. J. Reimel, M. van Lier-Walqui, and H. C. Morrison, 2022: Dual-Polarization Radar Fingerprints of Precipitation Physics: A Review. *Remote Sensing,* **14**, 3706 doi: 10.3390/rs14153706.

Kuster, C. M., B. R. Bowers, J. T. Carlin, T. J. Schuur, J. W. Brogden, R. Toomey, and A. Dean, 2021: Using KDP Cores as a Downburst Precursor Signature. *Wea. Forecasting*, **36**, 1183–1198, doi: 10.1175/WAF-D-21-0005.1.

Kuster, C. M. and Coauthors, 2025: Results from the Hazardous Weather Testbed: What do Forecasters Think About Dual-Polarization Phased Array Radar? NOAA/NSSL Technical Memo, 40 pp., https://doi.org/10.25923/p7m5-gm39.

Mahalik, M. C., B. R. Smith, K. L. Elmore, D. M. Kingfield, K. L. Ortega, and T. M. Smith, 2019: Estimates of Gradients in Radar Moments Using a Linear Least Squares Derivative Technique. *Wea. Forecasting*, **34**, 415–434, doi: 10.1175/WAF-D-18-0095.1.

Markowski, P. M., and Y. P. Richardson, 2017: Large Sensitivity of Near-Surface Vertical Vorticity Development to Heat Sink Location in Idealized Simulations of Supercell-Like Storms. *J. Atmos. Sci.*, **74**, 1095–1104, https://doi.org/10.1175/JAS-D-16-0372.1.

Torres, S. M., and Coauthors, 2016: Adaptive-weather-surveillance and multifunction capabilities of the National Weather Radar Testbed phased array radar. *Proc. IEEE*, **104**, 660–672, doi: 10.1109/JPROC.2015.2484288.

Torres, S. M. and D. Wasielewski, 2022: The Advanced Technology Demonstrator at the National Severe Storms Laboratory: Challenges and successes. IEEE Radar Conference, New York City, NY, IEEE, 1-6, doi: 10.1109/RadarConf2248738.2022.9764231.

Torres, S. M., C. D. Curtis, R. J. Estes, and S. B. Gregg, 2026: Adaptive Focused Observations on the Advanced Technology Demonstrator Phased-Array Radar, *IEEE Transactions on Radar Systems*, **4**, 463-472, https://doi.org/10.1109/TRS.2026.3656643.

Tuftedal, K. S., M. M. French, D. M. Kingfield, and J. C. Snyder, 2021: Observed Bulk Hook Echo Drop Size Distribution Evolution in Supercell Tornadogenesis and Tornadogenesis Failure. *Mon. Wea. Rev.*, **149**, 2539–2557, https://doi.org/10.1175/MWR-D-20-0353.1.

Zrnić, D., and Coauthors, 2007: Agile-beam phased array radar for weather observations. *Bull. Amer. Meteor. Soc.*, **88**, 1753–1766, doi: 10.1175/BAMS-88-11-1753.

Appendix 1: List of Case Details

Date	Case Type	Start Time (UTC)	End Time (UTC)	VCP Time/ Date	VCP Name	Sector Time/ Date	Sector Left Edge	Sector Right Edge
1/9	Winter Weather	1/9 14:27	1/9 22:53	1/9 14:37	Playlist: Winter Wx PPI Volume and Raster RHIs	1/9 14:37	144.5	234.5
1/29	Multicell Convection (Non-Severe)	1/29 19:18	1/29 22:20	1/29 19:18	Playlist: PAMST LDR QLCS 100+km and RHI Fast	1/29 19:18	180	270
2/12	Winter Weather	2/12 08:48	2/12 09:30	2/12 08:48 2/12 09:22 2/12 09:30	Playlist: WinterWx PPI Volume and Raster RHIs QLCS_100_Fast Playlist: PAMST QLCS LDR 0.5 and QLCS_100	2/12 08:48 2/12 08:52 2/12 09:22 2/12 09:43	225 180 135 115	315 270 225 205
2/18	Winter Weather	2/18 14:21	2/19 02:22	2/18 14:21	Playlist: WinterWx PPI Volume and Raster RHIs	2/18 14:21 2/18 18:40 2/18 18:57 2/18 19:37 2/18 23:30 2/18 23:35 2/19 00:40 2/19 01:26 2/19 01:31 2/19 01:37	235 90 270 145 90 270 225 205 180 145	145 180 360 235 180 360 315 295 270 235

						2/19 01:57	115	205
3/4	QLCS (Tornadic)	3/4 03:17	3/4 08:06	3/4 03:15 3/4 06:43 3/4 06:59 3/4 07:13	Playlist: PAMST QLCS_100 and Compare Playlist: QLCS_75-100 and Compare Playlist: QLCS_50-75 and Compare Playlist: QLCS_50 and Compare	3/4 03:15 3/4 05:22 3/4 05:43 3/4 07:28	225 235 220 210	315 285 310 300
3/8	Multicell Convection (Non-Severe)	3/8 18:35	3/8 19:20	3/8 18:35	Playlist: WinterWx PPI Volume and Raster RHIs	3/8 18:35 3/8 18:41	200 180	290 270
3/14	Fire	3/14 17:59	3/14 22:40	3/14 17:59	Playlist: PAMST Fire Wx	3/14 17:59 3/14 18:01 3/14 18:22 3/14 18:48 3/14 19:04 3/14 19:17 3/14 19:25 3/14 19:56 3/14 20:05 3/14 21:16 3/14 21:29 3/14 21:34	225 255 285 293 85 225 85 293 75 180 170 160	325 345 15 23 175 315 175 23 165 270 260 250
3/17	Fire	3/17 20:43	3/17 21:21	3/17 20:43	Playlist: PAMST Fire Wx	3/17 20:43	295	25

3/30	Multicell Convection, QLCS (Severe)	3/30 02:05	3/30 05:57	3/30 02:05	Playlist: PAMST Supercell 100+km and RHI Fast	3/30 02:05	210	300
						3/30 02:06	200	290
						3/30 02:11	190	280
						3/30 02:22	175	265
				3/30 02:28	Playlist: PAMST Supercell 50-100km and RHI Fast			
						3/30 03:08	155	245
				3/30 03:09	Playlist: PAMST Supercell 0-50km and RHI Fast			
						3/30 03:18	145	235
						3/30 03:23	135	225
						3/30 03:27	125	215
						3/30 03:38	255	345
				3/30 03:40	Playlist: PAMST Supercell 50-100km and RHI Fast			
						3/30 04:08	265	355
						3/30 04:29	280	10
						3/30 04:40	290	20
						3/30 05:04	294	24
				3/30 05:06	Playlist: PAMST Supercell 0-50km and RHI Fast			
				3/30 05:34	Scan: Supercell_Fast_Degree_Spaced			
4/1	Supercell (Non-Tornadic)	4/1 21:10	4/2 01:30	4/1 21:10	Supercell_100km_Fast	4/1 21:10	225	315
						4/1 21:39	244	344
						4/1 21:58	264	354
						4/1 22:11	271	1
						4/1 22:42	287	377
						4/1 23:01	294	384
						4/1 23:43	169	259
						4/2 01:16	153	243
				4/2 01:19	PAMST Supercell 50-100km and RHI Fast			

4/2	QLCS (Non-Tornadic)	4/2 08:12	4/2 11:33	4/2 08:12 4/2 08:40 4/2 09:09 4/2 09:45 4/2 11:21	PAMST QLCS_100+km and RHI Fast PAMST QLCS_75_to_100km and RHI Fast PAMST QLCS_50to75km and RHI Fast PAMST QLCS_0to50km and RHI Fast PAMST QLCS_50to75km and RHI Fast	4/2 08:12 4/2 08:36 4/2 09:21 4/2 10:12 4/2 11:21	294 255 225 170 105	384 345 315 260 195
4/18	Supercell (Non-Tornadic)	4/18 21:53	4/19 05:18	4/18 21:53 4/18 22:47	Fire_Wx Playlist: Supercell LDR 0.5, Supercell Constant, and LDR RHI sector	4/18 21:46 4/18 23:39 4/19 01:30 4/19 01:50 4/19 02:02 4/19 02:43 4/19 03:01 4/19 03:26 4/19 03:37 4/19 04:02 4/19 04:33 4/19 04:39 4/19 05:03	180 225 128 110 95 85 70 85 105 145 165 195 295	270 315 218 200 185 175 160 175 195 235 255 285 25

4/24	QLCS (Tornadic)	4/24 08:40	4/24 10:33	4/24 08:40 4/24 08:59 4/24 09:26 4/24 10:04	PAMST QLCS_100+km and RHI Fast PAMST QLCS_75to100km and RHI Fast PAMST QLCS_50to75km and RHI Fast PAMST QLCS_0to50km and RHI Fast	4/24 08:40	188	278
4/25	QLCS (Tornadic)	4/25 03:37	4/25 05:37	4/25 03:37 4/25 04:34	Playlist: PAMST QLCS_100+km and RHI Fast Playlist: PAMST QLCS_75to100km and RHI Fast	4/25 03:37 4/25 05:05 4/25 05:28	270 275 270	360 5 360
4/28	Multicell Convection (Severe)	4/28 21:33	4/29 03:52	4/28 21:33	Supercell LDR 0.5, Const Range, LDR RHI Sector	4/28 21:33 4/28 23:39 4/29 02:28	180 200 220	270 290 310
4/29	Supercell, QLCS (Tornadic)	4/29 15:09	4/30 01:46	4/29/25 15:09	Playlist: Supercell LDR0.5, Cont Range, Sector RHIs	4/29 15:09 4/29 15:37 4/29 16:45 4/29 18:06 4/29 19:41 4/29 22:18 4/29 22:28	225 240 270 155 85 135 180	315 330 360 245 175 225 270
5/2	QLCS (Tornadic)	5/2 5:05	5/2 08:56	5/2 05:05 5/2 08:51	PAMST LDR QLCS_100+km and RHI Fast Playlist QLCS 50 and Compare	5/2 05:05 5/2 08:15 5/2 08:37	205 205 95	295 115 185

5/17	Supercell (Tornadic)	5/17 21:00	5/18 03:08	5/17 21:00	Supercell LDR 0.5, Const Range, LDR RHI Sector	5/17 21:00 5/17 21:48 5/17 22:00 5/17 22:20 5/17 22:35 5/17 22:55 5/18 02:07 5/18 02:28 5/18 02:52	180 145 125 110 95 85 275 285 293	270 235 215 200 185 175 5 15 23
5/19	Supercell, QLCS (Tornadic)	5/19 16:48	5/19 23:05	5/19 16:48 5/19 18:54 5/19 19:01	Playlist Supercell LDR 0.5, Const Range, and LDR Sector Fire Wx Playlist Supercell LDR 0.5, Const Range, and LDR Sector	5/19 16:48 5/19 17:02 5/19 17:13 5/19 17:15 5/19 17:17 5/19 17:18 5/19 17:40 5/19 18:02 5/19 18:18 5/19 18:54 5/19 18:59 5/19 19:11 5/19 19:17 5/19 19:50 5/19 20:48 5/19 21:17 5/19 21:18 5/19 21:22 5/19 21:23 5/19 21:28 5/19 21:30	170 145 125 110 100 85 135 105 85 180 135 115 90 85 165 190 193 198 200 205 210	260 235 215 200 190 175 225 195 195 270 225 205 180 175 255 280 283 288 290 295 300

				5/19 22:53 5/19 23:02	QLCS_100 and Compare QLCS_Compare	5/19 21:33 5/19 21:35 5/19 21:37 5/19 21:40 5/19 21:43 5/19 21:46 5/19 22:51	214 218 245 270 280 285 90	304 308 335 360 10 15 180
5/22	Supercell (Tornadic)	5/22 14:14	5/22 18:25	5/22 14:16	Supercell LDR 0.5, Const Range, LDR RHI Sector	5/22 14:14 5/22 14:51 5/22 16:00 5/22 16:39	225 115 105 100	135 205 195 190
5/29	Supercells (Non-Tornadic)	5/29 20:29	5/29 23:02	5/29 20:29	Supercell LDR0.5, Const Range, and Narrow LDR RHI	5/29 20:29 5/29 21:21 5/29 21:37 5/29 21:57 5/29 22:14 5/29 22:48 5/29 22:56	225 245 265 255 225 205 180	325 335 355 345 315 295 270
6/3 Day	MCS (Non-Severe)	6/3 02:18	6/3 04:01	6/3 02:18	Playlist: PAMST LDR QLCS_100+km and RHI Fast	6/3 02:18 6/3 03:33	245 255	335 345

6/3 Evening	Supercell, QLCS (Tornadic)	6/3 17:28	6/4 00:58	6/3 17:28	QLCS LDR 0.5, Const Range, LDR RHI Sector Playlist	6/3 17:28 6/3 18:28 6/3 18:37 6/3 20:23 6/3 20:34	245 270 295 250 240	335 360 205 340 330
				6/3 20:51	Supercell LDR 0.5, Const Range, LDR RHI Sector	6/3 20:53 6/3 20:54 6/3 21:23 6/3 21:38 6/3 22:35 6/3 23:17	355 20 340 260 35 85	265 290 70 350 125 175
6/5	Supercells (Non-Tornadic)	6/5 19:49	6/6 00:27	6/5 18:49	Supercell LDR 0.5, Const Range, LDR RHI Sector	6/5 18:49 6/5 21:54 6/5 21:59 6/5 22:05 6/5 22:15 6/5 22:25 6/5 22:30 6/5 22:35 6/5 23:09 6/5 23:38	225 230 240 225 215 205 185 175 130 90	315 320 330 315 305 295 275 265 220 180
6/6	QLCS (Tornadic)	6/6 09:14	6/6 12:48	6/6 10:52	QLCS LDR 0.5. Const Range, and LDR Sector	6/6 10:56 6/6 10:57	105 90	195 180

6/7	Supercell, QLCS (Tornadic)	6/7 03:07	6/7 09:09	6/7 03:07	Supercell LDR 0.5, Const Range, LDR RHI Sector	6/7 03:07 6/7 04:47 6/7 05:31 6/7 05:39 6/7 05:44 6/7 05:44 6/7 07:12 6/7 07:23 6/7 07:34 6/7 07:50 6/7 08:10 6/7 08:35 6/7 09:05	225 255 284 270 250 270 280 290 294 225 245 250 245	315 345 14 0 340 0 10 20 24 315 335 340 335
6/8	QLCS (Tornadic)	6/8 22:17	6/9 02:16	6/8 22:17	Supercell LDR 0.5, Const Range, LDR RHI Sector	6/8 22:17 6/9 00:34 6/9 01:23 6/9 01:33	265 240 265 135	355 330 355 225
6/18	QLCS (Tornadic)	6/18 03:33	6/18 04:34	6/18 03:33 6/18 04:15 6/18 04:21	QLCS LDR 0.5, Const Range, LDR RHI Sector Test_Super_Res_1 Downburst_25-50_Adv first and Downburst_25-50_Adv_MRLE	6/18 03:33 6/18 04:18 6/18 04:21	294 105 294	24 195 24
6/18 (part 2)	Multicell Convection (Downburst)	6/18 21:19	6/19 00:00	6/18 21:19 6/18 22:39	Supercell LDR 0.5, Const Range, LDR RHI Sector Downburst_75-100_Adv_MRLE	6/18 21:19	170	170
6/26	MCS, Multicell Convection (Downbursts)	6/26 19:53	6/26 23:10	6/26 19:53 6/26 20:41 6/26 21:11	Playlist: Downburst_75-100_Adv Playlist: Downburst_50-75_Adv Downburst_50-75_Adv Playlist	6/26 19:53 6/26 20:31 6/26 20:39 6/26 21:11	245 255 265 245	335 345 355 335

				6/26 21:27 6/26 21:51	Downburst_50-75_Adv_MRLE Playlist Downburst_25-50_Adv Playlist	 6/26 22:59	 205	 295
6/30	Multicell Convection (Downbursts)	6/30 19:50	6/30 23:01	6/30 19:50 6/30 21:22	Downburst_75-100_Adv Downburst_50-75_Adv	6/30 19:50 6/30 21:17 6/30 21:38 6/30 22:13 6/30 22:23	200 175 165 155 115	290 265 255 245 205
7/08	Multicell Convection (Downbursts)	7/8 19:48	7/8 22:50	7/8 19:59 7/8 21:27 7/8 22:04 7/8 22:25	Downburst_50-75_Adv Downburst_25-50_Adv Downburst_25-50_Adv_MRLE Downburst_50-75_Adv	7/8 19:59 7/8 22:12 7/8 22:17	295 235 255	25 325 345
7/09	Multicell Convection (Downbursts)	7/9 02:24	7/9 03:54	7/9 02:24 7/9 02:59	Downburst_50-75_Adv_MRLE Downburst_25-50_Adv_MRLE	7/9 02:24 7/9 03:38 7/9 03:46	285 270 245	15 0 335
7/12	Multicell Convection (Non-Severe)	7/12 19:23	7/12 20:15	7/12 19:23 7/12 19:26	combined_exp_beam_types Playlist: Downburst_25-50_Adv	7/12 19:23	180	270
8/11	Multicell Convection (Downbursts)	8/11 20:40	8/11 22:08	8/11 20:40 8/11 21:05	Downburst_25-50_Adv Playlist Downburst_25-50_Adv_MRLE Playlist	8/11 20:40	230	320
8/19	Multicell Convection (Downbursts)	8/19 17:59	8/20 00:51	8/19 17:59 8/19 18:10 8/19 20:20 8/19 22:33	Downburst_75-100_Adv Downburst_50-75_Adv Downburst_75-100_Adv Downburst_25-50_Adv	8/19 17:59 8/19 20:41 8/19 21:59	225 265 295	325 355 25

						8/20 00:18	180	270
8/26	Multicell Convection (Non-Severe)	8/26 15:33	8/26 18:23	8/26 15:33	QLCS LDR 0.5, Const Range, LDR RHI Sector	8/26 15:33 8/27 17:08	135 90	225 180
8/27	Multicell Convection (Non-Severe)	8/27 14:39	8/27 18:05	8/27 14:39 8/27 15:01	Playlist: QLCS LDR 0.5, Const Range, Narrow RHI Sector Playlist: QPE LDR0.5, Const Range, Raster Compare	8/27 14:39	295	25
8/28	Multicell Convection (Non-Severe)	8/28 13:37	8/28 14:52	8/28 13:37	QPE LDR0.5, ConstRange, Raster Compare Playlist	8/28 13:37 8/28 14:20 8/28 15:37	260 215 90	350 305 180
9/15	Multicell Convection (Non-Severe)	9/15 18:38	9/15 22:33	9/15 18:37 9/15 20:11	Downburst_75-100_Adv_MRLE Downburst_50-75_Adv_MRLE	9/15 18:37	235	325
9/16	Multicell Convection (Non-Severe)	9/16 19:18	9/16 22:13	9/16 19:18 9/16 20:12 9/16 21:28	Playlist: Downburst_25-50_Adv_Full Playlist: Downburst_50-75_Adv_Full Playlist: Downburst_75-100_Adv_Full	9/16 19:18 9/16 19:38 9/16 20:37 9/16 20:43	225 255 245 235	325 345 335 315
9/17	Multicell Convection (Non-Severe)	9/17 20:07	9/17 21:40	9/17 20:07 9/17 21:45	Playlist: QLCS LDR 0.5, Const Range, RHI Narrow Sector PAMST Self-Consistency 5x5	9/17 20:07	270	360
9/18	Multicell Convection (Non-Severe)	9/18 14:20	9/18 17:10	9/18 14:20	PAMST QLCS LDR0.5 and QLCS_50	9/18 14:20 9/18 14:36	180 270	270 360

11/20	Clear Air/Eng Test, Multicell Convection (Severe)	11/20 02:21	11/21 05:01	11/20 02:22	Unknown (due to a random error with note taking application)	11/20 02:22 11/20 02:25 11/20 02:59 11/20 04:20 11/20 04:39	180 210 265 225 265	270 300 355 315 355
12/4	Winter Weather	12/04 05:36	12/04 15:36	12/4 05:36 12/4 06:55 12/4 07:07 12/4 08:57 12/4 12:11	Playlist: WinterWx LDR New-Testing Playlist: WinterWx PPI Volume and Raster RHIs Playlist: Supercell LDR 0.5, Const Range, LDR RHI Sector Playlist: WinterWx LDR Sampling Playslist: PAMST QLCS_50to75	12/4 05:36	225	315